PNAS RESEARCH ARTICLE | PHARMACOLOGY

Natural variation in the binding pocket of a parasitic flatworm TRPM channel resolves the basis for praziquantel sensitivity

Claudia M. Rohr[a], Daniel J. Sprague[a], Sang-Kyu Park[a], Nicholas J. Malcolm[a], and Jonathan S. Marchant[a,1]

Edited by L. Sibley, Washington University in St. Louis, St. Louis, MO; received October 20, 2022; accepted November 11, 2022

The drug praziquantel (PZQ) is the key clinical therapy for treating schistosomiasis and other infections caused by parasitic flatworms. A schistosome target for PZQ was recently identified— a transient receptor potential ion channel in the melastatin subfamily ($TRPM_{PZQ}$)—however, little is known about the properties of $TRPM_{PZQ}$ in other parasitic flatworms. Here, $TRPM_{PZQ}$ orthologs were scrutinized from all currently available parasitic flatworm genomes. $TRPM_{PZQ}$ is present in all parasitic flatworms, and the consensus PZQ binding site was well conserved. Functional profiling of trematode, cestode, and a free-living flatworm $TRPM_{PZQ}$ ortholog revealed differing sensitives (~300-fold) of these $TRPM_{PZQ}$ channels toward PZQ, which matched the varied sensitivities of these different flatworms to PZQ. Three loci of variation were defined across the parasitic flatworm $TRPM_{PZQ}$ pocketome with the identity of an acidic residue in the TRP domain acting as a gatekeeper residue impacting PZQ residency within the $TRPM_{PZQ}$ ligand binding pocket. In trematodes and cyclophyllidean cestodes, which display high sensitivity to PZQ, this TRP domain residue is an aspartic acid which is permissive for potent activation by PZQ. However, the presence of a glutamic acid residue found in other parasitic and free-living flatworm $TRPM_{PZQ}$ was associated with lower sensitivity to PZQ. The definition of these different binding pocket architectures explains why PZQ shows high therapeutic effectiveness against specific fluke and tapeworm infections and will help the development of better tailored therapies toward other parasitic infections of humans, livestock, and fish.

parasitic flatworm | Ca^{2+} signaling | TRP channel

Significance

The drug praziquantel has been used for decades to treat infections caused by parasitic flatworms, including schistosomiasis which afflicts over 200 million people worldwide. Most flukes and tapeworms display high sensitivity to praziquantel; however, the molecular basis for the unique sensitivity of some, but not all, parasites to praziquantel is unclear. Here, we comprehensively analyzed sequence variation in the binding pocket of a flatworm ion channel target of praziquantel, known as $TRPM_{PZQ}$, and define a key residue that underpins the exquisite sensitivity of trematode and certain cestodes to praziquantel. This insight provides impetus for designing new drugs that treat various parasitic flatworm infections where treatments are currently lacking or where improvements over praziquantel could be realized.

Praziquantel (PZQ), a drug discovered in the 1970s, has been in clinical usage for four decades to treat many different diseases caused by parasitic flatworms (1). Notably, PZQ is the key clinical agent for treating the neglected tropical disease schistosomiasis, which afflicts over 200 million people worldwide (2, 3). PZQ is classified as an essential medication by the World Health Organization and is integral to the current roadmap of interventions that are designed to control schistosomiasis morbidity and eliminate schistosomiasis as a public health problem.

PZQ effects an immediate paralysis of schistosome worms in vitro with concomitant surface damage that facilitates immunological clearance of worms in vivo (1, 4, 5). Despite the long-term clinical use of PZQ as an anthelminthic drug, the flatworm target of PZQ has remained undefined. However, a prime candidate was recently identified in *Schistosoma mansoni*: a Ca^{2+}-permeable ion channel of the transient receptor potential melastatin family named *Schistosoma mansoni* $TRPM_{PZQ}$ (*Sm*.$TRPM_{PZQ}$, (6)). Heterologous expression of *Sm*.$TRPM_{PZQ}$ in mammalian cells conferred responsiveness to PZQ, with PZQ elevating cytoplasmic Ca^{2+} with an observed sensitivity in the submicromolar range and stereoselectivity toward the active enantiomer (*R*)-PZQ. These features match the known action of PZQ on intact worms (7). Subsequent work validated *Sm*.$TRPM_{PZQ}$ as a relevant in vivo flatworm target of PZQ, based on more comprehensive pharmacological and genetic analyses of *Sm*.$TRPM_{PZQ}$ properties (8, 9).

In addition to treating schistosomiasis, PZQ also displays a broad spectrum activity against other parasitic flatworm infections, including diseases caused by other trematodes, monogeneans, and cestodes (1, 5, 10–12). However, PZQ sensitivity of these parasitic flatworms is not identical leading to different clinical dosages required to effectively treat different infections (13–15). PZQ also has effects on free-living flatworms (16–18) but over a much higher concentration range (tens of micromolar) than active against schistosomes and certain tapeworms (hundreds of nanomolar).

Variation in $TRPM_{PZQ}$ binding pocket sequences may account for the varied sensitivities of different flatworms to PZQ. Precedent for this explanation has been established by comparison of a PZQ-sensitive (*S. mansoni*) and a PZQ-insensitive (*Fasciola hepatica*) parasitic flatworm. The binding pockets of these $TRPM_{PZQ}$ orthologs harbored a single amino acid difference at a residue (N1388 in *S. mansoni*, T1270 in *F. hepatica*) within the

Author contributions: C.M.R., D.J.S., S.-K.P., and J.S.M. designed research; C.M.R., D.J.S., and S.-K.P. performed research; N.J.M. contributed new reagents/analytic tools; C.M.R., D.J.S., and S.-K.P. analyzed data; and C.M.R., D.J.S., S.-K.P., and J.S.M. wrote the paper.

The authors declare no competing interest.

This article is a PNAS Direct Submission.

[1]To whom correspondence may be addressed. Email: JMarchant@mcw.edu.

This article contains supporting information online at https://www.pnas.org/lookup/suppl/doi:10.1073/pnas.2217732120/-/DCSupplemental.

Published December 27, 2022.

first transmembrane helix (S1) of the voltage sensor-like domain (VSLD) of the ion channel (8). This residue was predicted to engage the cyclohexyl carbonyl of PZQ *via* hydrogen bonding (8). Reciprocal mutations caused either a loss (N1388T in *Sm.*$TRPM_{PZQ}$) or gain (T1270N in *Fh.*$TRPM_{PZQ}$) of sensitivity to PZQ (8). Natural sequence variation within the $TRPM_{PZQ}$ binding pocket, therefore, underpins the insensitivity of *Fh.* $TRPM_{PZQ}$ to PZQ, correlating with the loss of PZQ activity against *F. hepatica*. The refractoriness toward PZQ has necessitated the development of other approaches to combat human and agricultural infections caused by this liver fluke (19, 20).

This example provides impetus for a comprehensive evaluation of $TRPM_{PZQ}$ binding pocket architecture across all parasitic flatworms. This analysis, performed in this study, revealed the following: first, a molecular basis for the uniquely high sensitivity of certain flukes and tapeworms to PZQ, long recognized as a key feature of PZQ action; second, examples where the interaction of PZQ with $TRPM_{PZQ}$ is nonoptimal identifying opportunity to develop new ligands to better treat specific parasitic infections.

Results

PZQ Activation of Schistosome $TRPM_{PZQ}$ Channels. As PZQ is a broadly used clinical therapy for treating parasitic flatworm infections (1), it is important to define whether other $TRPM_{PZQ}$ orthologs are also sensitive to PZQ. For example, while three schistosome species—*S. mansoni*, *Schistosoma haematobium,* and *Schistosoma japonicum*—are responsible for most human infections worldwide, only *Sm.*$TRPM_{PZQ}$ has been studied to date (6, 8).

S. haematobium $TRPM_{PZQ}$ was cloned from a cDNA sample prepared from *S. haematobium* total RNA (see *Methods*), to yield a full-length sequence for *Sh.*$TRPM_{PZQ}$ of 2195 amino acids (*SI Appendix*, Fig. S1). Based on the sequences of *Sm.*$TRPM_{PZQ}$ and *Sh.*$TRPM_{PZQ}$, a full-length sequence for *Sj.*$TRPM_{PZQ}$ (2179 amino acids) was synthesized from the *S. japonicum* genomic annotation (*SI Appendix*, Fig. S1). The three *Schistosoma spp.* $TRPM_{PZQ}$ orthologs were highly similar in sequence (>80% amino acid identity, *SI Appendix*, Table S1). The individual schistosome $TRPM_{PZQ}$ channels were transiently expressed in HEK293 cells, and their responsiveness to the PZQ enantiomers, (*R*)-PZQ and (*S*)-PZQ, was examined by monitoring fluorescence changes using a cytoplasmic Ca^{2+}-sensitive dye. The addition of (*R*)-PZQ to cells expressing individual schistosome $TRPM_{PZQ}$ channels caused a rapid increase in cytoplasmic Ca^{2+}, whereas no Ca^{2+} increase was seen in control cells (Fig. 1*A*). Activation of each of these channels displayed stereoselectivity for (*R*)-PZQ over (*S*)-PZQ (Fig. 1*A*), consistent with the effects of individual PZQ enantiomers on worms in vitro and in vivo (21). The observed sensitivities to (*R*)-PZQ were EC_{50} = 221 ± 85 nM for *Sh.*$TRPM_{PZQ}$, EC_{50} = 234 ± 80 nM for *Sj.*$TRPM_{PZQ}$, and EC_{50} = 281 ± 29 nM for *Sm.*$TRPM_{PZQ}$ (Fig. 1 *B–D*).

(*R*)-PZQ has been shown to activate *Sm.*$TRPM_{PZQ}$ via engagement of a binding pocket located at the base of the VSLD of the ion channel (8). This PZQ binding pocket of $TRPM_{PZQ}$ is formed

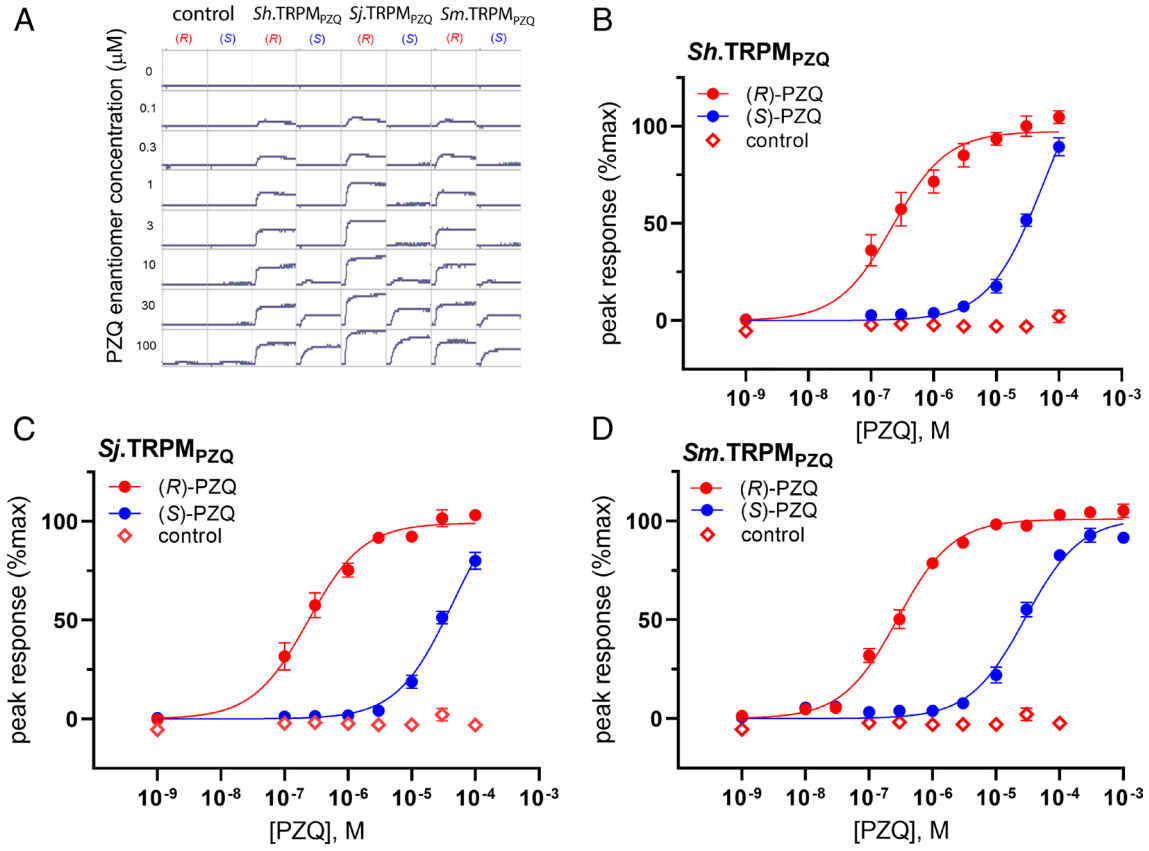

Fig. 1. Functional profiling of schistosome $TRPM_{PZQ}$ channels. (*A*) Examples of real-time fluorescence values from a representative experiment that depict the effects of (*R*)-PZQ (red) and (*S*)-PZQ (blue) in untransfected cells ('control') as well as HEK293 cells expressing *Sh.*$TRPM_{PZQ}$, *Sj.*$TRPM_{PZQ}$, and *Sm.*$TRPM_{PZQ}$. PZQ enantiomers (concentrations on left hand side) were added after ~20 s of sampling a baseline fluorescence emission. (*B–D*) Concentration–response relationships for the activation of (*B*) *Sh.*$TRPM_{PZQ}$, (*C*) *Sj.*$TRPM_{PZQ}$, and (*D*) *Sm.*$TRPM_{PZQ}$ by PZQ enantiomers, (*R*)-PZQ (red) and (*S*)-PZQ (blue). (±)-PZQ was also profiled against untransfected cells (open symbols). Data are expressed as a percentage of the maximum response evoked by (*R*)-PZQ at *Sm.*$TRPM_{PZQ}$ and represent the mean ± SEM of n ≥ 3 independent experiments.

by residues from each of the first four transmembrane spanning helices (S1 to S4), their interconnecting loops, and the juxtamembrane TRP helix. Based on the understanding of how (*R*)-PZQ engages this binding pocket, point mutants of a key asparagine residue in the first transmembrane helix (S1) were made in *Sh*.$TRPM_{PZQ}$ (*Sh*.$TRPM[N1314A]_{PZQ}$) and *Sj*.$TRPM_{PZQ}$ (*Sj*.$TRPM[N1299A]_{PZQ}$). This S1 asparagine is important for hydrogen bonding to (*R*)-PZQ in *Sm*.$TRPM_{PZQ}$ (8). Ligand sensitivity was reduced in these mutants, such that (±)-PZQ (10 μM) caused little activity relative to the wildtype construct (peak response of 7.7 ± 5.9% for *Sh*.$TRPM[N1314A]_{PZQ}$, 0.7 ± 1.3% for *Sj*.$TRPM[N1299A]_{PZQ}$ and 1.9 ± 1.5% for *Sm*.$TRPM[N1388A]_{PZQ}$). These data suggest a similar mechanism of PZQ engagement by each of the schistosome $TRPM_{PZQ}$ orthologs.

A total of 23 amino acids project within a 5Å radius of the PZQ binding pose (Fig. 2*A*), providing an approximation of the binding pocket 'lining' (8). Using these 23 residues as a barcode that encodes PZQ sensitivity, the identity of amino acids at equivalent positions within $TRPM_{PZQ}$ orthologs from all other schistosome species was scrutinized. Bioinformatic analysis extended to eight other *Schistosoma spp*. $TRPM_{PZQ}$ sequences revealed the complete conversation of residues lining the PZQ binding pocket across all the Schistosomatidae (*SI Appendix*, Table S2). This analysis encompassed the three species that were functionally profiled (*S. mansoni, S. haematobium,* and *S. japonicum*), four other schistosome species (*S. bovis, S. curassoni, S. mattheei,* and *S. margrebowiei*), as well as the avian schistosome *Trichobilharzia regenti*, which causes cercarial dermatitis (swimmer's itch) in humans (22). The conservation of the PZQ binding pocket in all schistosome $TRPM_{PZQ}$ channels is consistent with the in vitro sensitivity to PZQ reported in each of these species and the known efficacy of PZQ for treating human, livestock, and wild animal schistosome infections (1, 3, 13, 22, 23).

PZQ Activation of Other Trematode $TRPM_{PZQ}$ Orthologs. $TRPM_{PZQ}$ sequence information from other trematodes was then collated (*SI Appendix*, Table S2). Across all trematode $TRPM_{PZQ}$ sequences, the twenty-three residues lining the PZQ binding pocket were highly conserved (*SI Appendix*, Table S2), with the exception of *Fasciola spp*. The conservation of the binding pocket sequence would suggest that, with the exception of *Fasciola spp*., PZQ sensitivity is retained across all trematodes.

To test this prediction, several trematode $TRPM_{PZQ}$ orthologs were functionally profiled. Each of these trematode $TRPM_{PZQ}$ orthologs exhibited high sensitivity to (*R*)-PZQ (Fig. 2 *C*–*E*). These were $TRPM_{PZQ}$ from *Clonorchis sinensis* (the 'oriental liver fluke', EC_{50} = 193 ± 110 nM for (*R*)-PZQ at *Cs*.$TRPM_{PZQ}$), *Opisthorchis viverrini* (the 'Southeast Asian liver fluke', EC_{50} = 129 ± 52 nM for *Ov*.$TRPM_{PZQ}$), and *Echinostoma caproni* (EC_{50} = 90 ± 31 nM for *Ec*.$TRPM_{PZQ}$), Fig. 2 *C*–*E*). This is consistent with the known sensitivity of each of these parasites to PZQ in vitro (25) and the efficacy of PZQ in treating clinical diseases caused by these agents (1, 10). Bioinformatic analyses of the remaining trematode $TRPM_{PZQ}$ binding pockets (*Paragonimus spp*. and *Dicrocoelium dendriticum, Fasciolopsis buski*) revealed conservation of these binding pocket residues, again consistent with the known sensitivity of these flukes to PZQ (25–31).

The Fasciolidae provided the only example where the sequence of the PZQ binding pocket showed variation from the schistosome consensus (Fig. 2*B*). Both *F. hepatica* and *F. gigantica* harbored a threonine residue in S1 where an asparagine residue is present in all other digeneans. For *F. hepatica*, the presence of this S1 threonine residue rendered *Fh*.$TRPM_{PZQ}$ insensitive to PZQ (8), consistent with the lack of efficacy of PZQ against *F. hepatica* in vitro and in vivo. Here, *Fasciola gigantica* $TRPM_{PZQ}$ (*Fg*.$TRPM_{PZQ}$) was examined. The addition of (*R*)-PZQ did not increase cytoplasmic Ca^{2+} in cells expressing wild-type *Fg*.$TRPM_{PZQ}$ (Fig. 2*F*). Wild-type *Fg*.$TRPM_{PZQ}$ was refractory to PZQ, consistent with the known lack of efficacy of PZQ against *F. gigantica* (32). A mutant of wild-type *Fg*.$TRPM_{PZQ}$ to mimic the schistosome $TRPM_{PZQ}$ binding pocket consensus (*Fg*.$TRPM[T1271N]_{PZQ}$) was generated. In cells expressing *Fg*.$TRPM[T1271N]_{PZQ}$, (*R*)-PZQ evoked a concentration-dependent increase in Ca^{2+} (EC_{50} = 155 ± 30 nM).

In summary, analysis of 22 trematode $TRPM_{PZQ}$ orthologs revealed, with the exception of the *Fasciola spp*., a complete sequence conservation of the PZQ binding pocket (Fig. 2*B*). Functional profiling of $TRPM_{PZQ}$ orthologs, with the exception of the two *Fasciola spp*., showed stereoselective activation by (*R*)-PZQ. These data are consistent with the known sensitivity of trematode parasites to PZQ in vitro and in vivo and $TRPM_{PZQ}$ serving as a relevant in vivo target for PZQ.

PZQ Activation of Other Flatworm $TRPM_{PZQ}$ Orthologs. Bioinformatic analysis was extended to a total of 43 parasitic flatworm $TRPM_{PZQ}$ sequences. This analysis encompassed 35 different parasitic flatworm genomes currently aggregated on the WormBase ParaSite portal (33) and 8 examples where $TRPM_{PZQ}$ sequences have been annotated in other genomic datasets (*SI Appendix*, Table S2). $TRPM_{PZQ}$ orthologs were identifiable in every parasitic flatworm genome analyzed (6). *SI Appendix*, Table S2 collates the predicted PZQ binding pocket residues across all these $TRPM_{PZQ}$ orthologs, encompassing all available parasitic flatworm $TRPM_{PZQ}$ sequences, three free-living flatworm $TRPM_{PZQ}$ representatives (*Macrostomum lignano*, *Schmidtea mediterranea,* and *Dugesia japonica*) and the human TRPM2 and TRPM8 channels with which $TRPM_{PZQ}$ displays some domain homology (*SI Appendix*, Table S2). The 23 residues lining the VSLD binding pocket were well conserved across all the parasitic flatworm representatives, with only three positions showing variation from the trematode $TRPM_{PZQ}$ binding pocket consensus (Fig. 3*A*). The extent of variation at these positions is shown in Fig. 3*B* and *SI Appendix*, Table S2.

The first residue exhibiting variation was the previously characterized S1 residue (Fig. 3 *A* and *B*). This S1 binding pocket residue—represented by asparagine residue in all trematodes (with the exception of *Fasciola spp*.)—was represented by histidine in all cestodes as well as monopisthocotylean monogeneans. The second variant residue was in the S4–S5 loop (Fig. 3 *A* and *B*) which was represented by a threonine in *Sm*.$TRPM_{PZQ}$ (T1518) but as a serine in cyclophyllidean cestodes and an isoleucine in *M. lignano*. The final position showing variation was within the TRP helix (Fig. 3 *A* and *B*) where an aspartic acid residue in *Sm*.$TRPM_{PZQ}$ (D1677) was represented by a glutamic acid residue in monogeneans, pseudophyllidean cestodes, and free-living flatworms.

Therefore, three unique, natural $TRPM_{PZQ}$ binding pocket configurations were resolved in parasitic flatworms that diverged from the 'NTD' configuration seen in trematodes (Fig. 3*B*). These configurations were 'HSD' (variation underlined) in cyclophyllidean cestodes, 'HTE' in pseudophyllidean cestodes and *Gyrodactylus spp*. (monopisthocotylean monogeneans), and 'NTE' in *Protopolystoma xenopodis* (the sole polyopisthocotylean monogenean represented). The binding pocket consensus was less conserved in free-living planarians, with six amino acid differences observed between the *Dugesia japonica* and *Schmidtea mediterranea* $TRPM_{PZQ}$ binding pocket with *Sm*.$TRPM_{PZQ}$ (*SI Appendix*, Table S2). However, the $TRPM_{PZQ}$ pocket of free-living flatworm

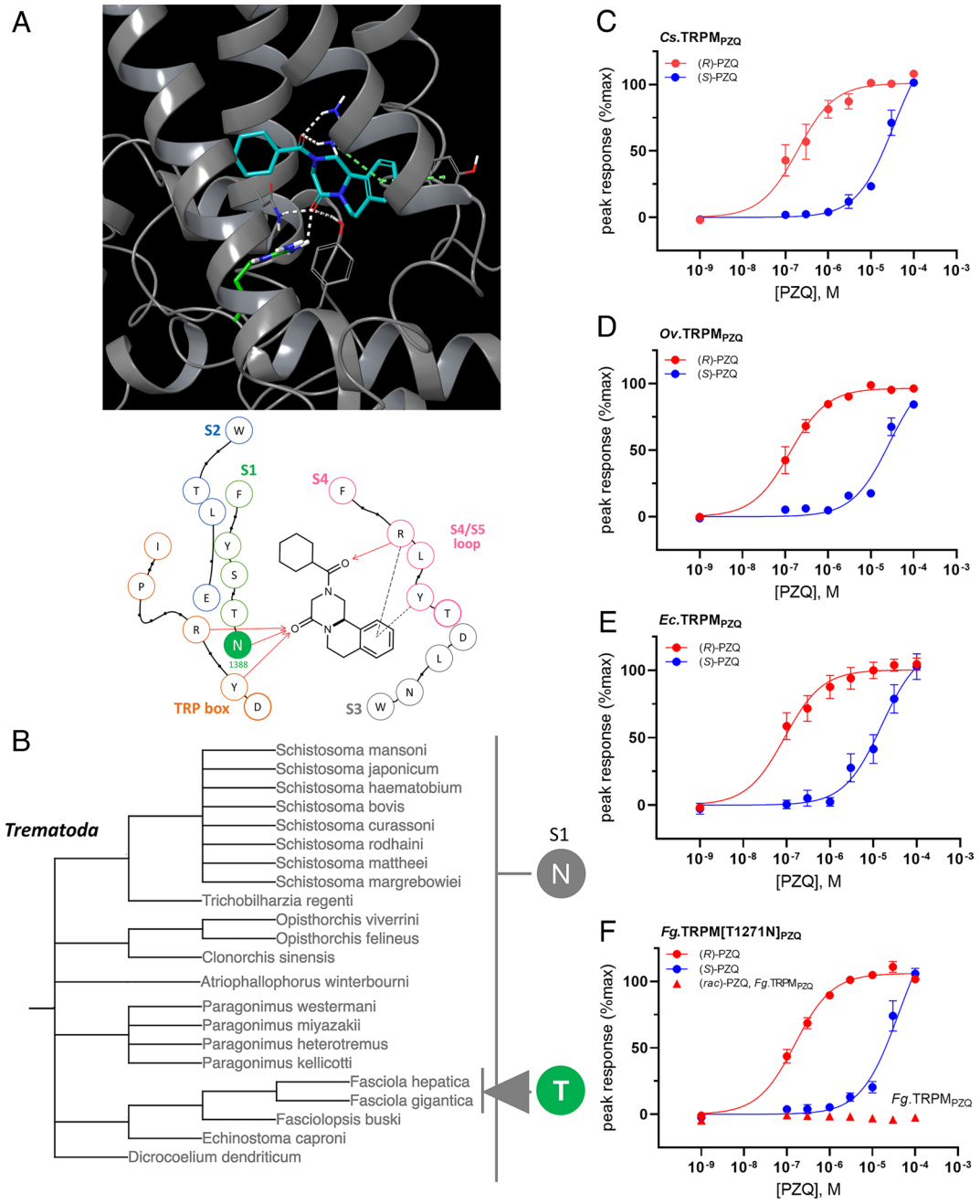

Fig. 2. $TRPM_{PZQ}$ binding pocket variation and functionality in trematode flatworms. (*A*) Top, docking pose of (*R*)-PZQ (blue) within the VSLD of *Sm*.$TRPM_{PZQ}$. Key interactions are shown as follows: hydrogen bond (white) and π–π stacking and cation–π interactions (dashed green line). Residue N1388 (S1) is shown in green. *Bottom*, interaction map of (*R*)-PZQ within the transmembrane binding pocket of *Sm*.$TRPM_{PZQ}$, showing residues within a 5Å radius of the proposed binding pose, modified from (8). Residues are colored to indicated channel domains (S1 to S4 and TRP domain). The asparagine residue shown in solid color—'N' (S1, green)—represents the location of variation within *Fasciola* spp. $TRPM_{PZQ}$. Interactions are highlighted as follows (hydrogen binding, arrows; cation–π, long dash; π–π, short dash). (*B*) Summary of sequence variation across parasitic trematode $TRPM_{PZQ}$ orthologs. The presented classification is reconstructed from the evolutionary pedigree of Lifemap (24) and is not a bootstrapped phylogeny. The *Fasciola* spp. threonine variant ('T') within the S1 helix is highlighted. (*C*–*F*) Concentration–response relationships for (*R*)-PZQ (red) and (*S*)-PZQ (blue) profiled against (*C*) *Clonorchis sinensis* (*Cs*.$TRPM_{PZQ}$), (*D*) *Opisthorchis viverrini* (*Ov*.$TRPM_{PZQ}$), (*E*) *Echinostoma caproni* $TRPM_{PZQ}$ (*Ec*.$TRPM_{PZQ}$) and (*F*) *Fasciola gigantica* $TRPM_{PZQ}$ (*Fg*.$TRPM_{PZQ}$, up triangle) and *Fg*.$TRPM[T1271N]_{PZQ}$ (circles). Data are expressed as mean ± SEM from n = 3 independent transient transfections of HEK293 cells.

Macrostomum lignano exhibited only two amino acid changes from the *Sm*.$TRPM_{PZQ}$ sequence, which were an isoleucine in the S4 to S5 loop as well as the glutamic acid residue in the TRP domain ('NIE' configuration). Human TRPM2 (5 differing residues) and TRPM8 (10 differing residues) exhibited greater divergence.

PZQ sensitivity was then assessed in several of these $TRPM_{PZQ}$ orthologs. These included $TRPM_{PZQ}$ from the cyclophyllidean cestodes *Echinococcus granulosus* (*Eg*.$TRPM_{PZQ}$) and *Mesocestoides corti* (*Mc*.$TRPM_{PZQ}$), as well as $TRPM_{PZQ}$ from a free-living flatworm representative, *M. lignano* (*Ml*.$TRPM_{PZQ}$). Both cestode channels exhibited high sensitivity to (*R*)-PZQ (EC_{50} = 55 ± 6 nM for *Eg*.$TRPM_{PZQ}$ and EC_{50} = 82 ± 3 nM for *Mc*.$TRPM_{PZQ}$, Fig. 3*C*), consistent with the known activity of PZQ against *E. granulosus*, *M. corti* and other cyclophyllidean cestodes (1, 15, 34, 35). *Ml*.$TRPM_{PZQ}$ was also activated by (*R*)-PZQ but displayed considerably lower sensitivity (EC_{50} = 18 ± 0.8 μM, Fig. 3*D*) but a sensitivity consistent with PZQ action on *M. lignano* (18). These data evidence a broad range in (*R*)-PZQ sensitivity (~330-fold) between these flatworm $TRPM_{PZQ}$ orthologs.

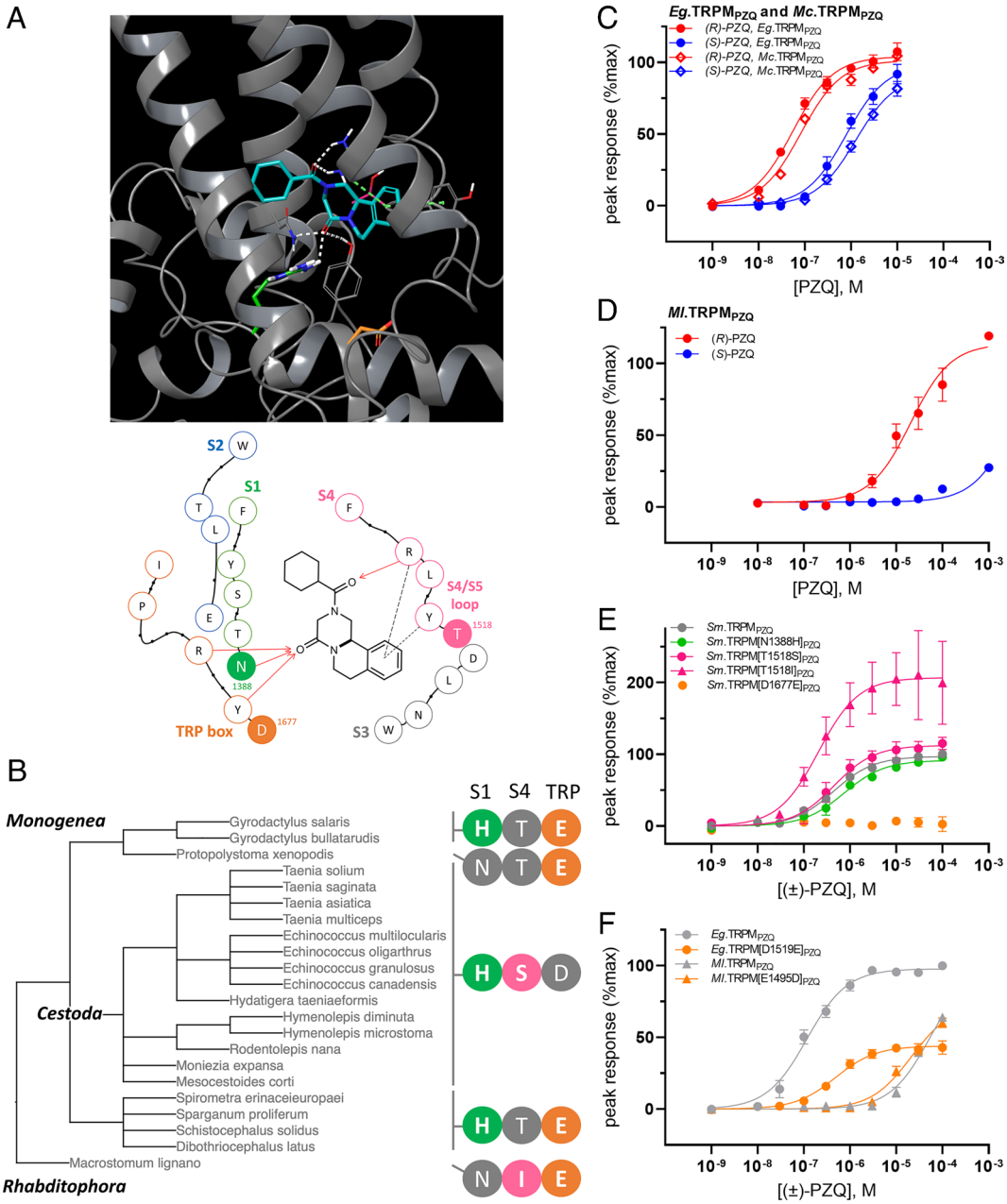

Fig. 3. Variation in the binding pocket and functional sensitivity of $TRPM_{PZQ}$ in other parasitic flatworms. (*A*, *Top*) docking pose of (*R*)-PZQ (blue) within the VSLD of *Sm*.$TRPM_{PZQ}$. Key interactions are shown as follows: hydrogen bond (white) and π–π stacking and cation–π interactions (dashed green line). Residues N1388 (S1, green), D1677 (TRP helix, orange) and T1518 (S4/S5 loop, pink) are highlighted. (*Bottom*) Interaction map of (*R*)-PZQ within the transmembrane binding pocket of *Sm*.$TRPM_{PZQ}$ as detailed in Fig. 2*A*. The residues in solid color: 'N' (S1, green), 'T' (S4/S5 loop, magenta), and 'D' (TRP box, orange) highlight the three sites of variation between wild-type $TRPM_{PZQ}$ sequences of parasitic flatworms. (*B*) Summary of sequence variation in $TRPM_{PZQ}$ orthologs using a classification reconstructed from Lifemap (24). Binding pocket sequence combinations define two cestode groupings ('HSD' vs 'HTE', cyclophyllidean versus pseudophyllidean cestodes), and two groupings of monogeneans ('HTE' vs 'NTE', monopisthocotylean versus polyopisthocotylean monogeneans). The sequence from a free-living flatworm representative (*Macrostomum lignano*) is also shown ('NIE'). (*C*) Concentration–response curve for activation of *Echinococcus granulosus* $TRPM_{PZQ}$ (*Eg*.$TRPM_{PZQ}$) and *Mesocestoides corti* $TRPM_{PZQ}$ (*Mc*.$TRPM_{PZQ}$) by (*R*)-PZQ (red) and (*S*)-PZQ (blue). (*D*) Concentration–response curve for the activation of *Macrostomum lignano* $TRPM_{PZQ}$ (*Ml*.$TRPM_{PZQ}$) by PZQ enantiomers, (*R*)-PZQ (red) and (*S*)-PZQ (blue). (*E*) Concentration–response relationships for four different point mutants made within the full-length *Sm*.$TRPM_{PZQ}$ backbone (*Sm*.$TRPM[N1388H]_{PZQ}$, *Sm*.$TRPM[T1518S]_{PZQ}$, *Sm*.$TRPM[T1518I]_{PZQ}$, and *Sm*.$TRPM[D1677E]_{PZQ}$) expressed relative to the maximal response of the wild-type *Sm*.$TRPM_{PZQ}$ sequence. (*F*) Effects of mutation of the natural TRP helix acidic residue in wild-type *Eg*.$TRPM_{PZQ}$ ('*D*' to '*E*', orange circle) and *Ml*.$TRPM_{PZQ}$ ('*E*' to '*G*', orange triangle). Data are expressed as mean ± SEM from n = 3 independent transfections.

Molecular Basis for Varied PZQ Sensitivity. To investigate the basis for this differential sensitivity, we examined the functional impact of mutants at each of the three identified binding pocket residues that show natural variation. Mutations were generated in *Sm*.$TRPM_{PZQ}$ (*Sm*.$TRPM[N1388H]_{PZQ}$, *Sm*.$TRPM[T1518S]_{PZQ}$, *Sm*.$TRPM[T1518I]_{PZQ}$, and *Sm*.$TRPM[D1677E]_{PZQ}$, Fig. 3*E*), and each was functionally profiled using the Ca^{2+} reporter assay. Two mutants—*Sm*.$TRPM[N1388H]_{PZQ}$ and *Sm*.$TRPM[T1518S]_{PZQ}$—exhibited equivalent sensitivity toward PZQ as the wild-type channel (Fig. 3*E*). One mutant—*Sm*.$TRPM[T1518I]_{PZQ}$—displayed higher sensitivity (EC_{50} = 207 ± 27 nM) than the wild-type channel (EC_{50} = 442 ± 55 nM, Fig. 3*E*). However, *Sm*.$TRPM[D1677E]_{PZQ}$ displayed no responsiveness to (±)-PZQ (Fig. 3*E*).

With the clear caveat that these point mutations were all made within the *S. mansoni* $TRPM_{PZQ}$ binding pocket and not in the context of full-length sequences of the different $TRPM_{PZQ}$

orthologs, the results suggest that PZQ sensitivity is retained at naturally occurring S1 ('H') and S4 variants ('S' and 'I'). However, the acidic residue substitution in the TRP domain (from aspartic acid 'D' to glutamic acid 'E') markedly impaired PZQ action. The presence of the glutamic acid residue was also associated with poor sensitivity to PZQ in *Ml*.TRPM$_{PZQ}$ (Fig. 4*D*) where this glutamic acid residue occurs naturally (Fig. 3*D*). The importance of this TRP helix acidic residue was also highlighted by reciprocal mutagenesis. Introduction of a ('D' to 'E') point mutant within the backbone of the cestode TRPM$_{PZQ}$ channel lowered (±)-PZQ sensitivity by ~4-fold (EC_{50} for (±)-PZQ = 485 ± 51nM in *Eg*. TRPM[D1519E]$_{PZQ}$ versus 116 ± 20 nM in wild-type *Eg*. TRPM$_{PZQ}$, Fig. 3*F*). Reciprocally, the introduction of a ('E' to 'D') point mutant in the *Ml*.TRPM$_{PZQ}$ channel increased (±)-PZQ sensitivity by ~2.5-fold (EC_{50} for (±)-PZQ = 21.1 ± 3.1 µM in *Ml*. TRPM[E1495D]$_{PZQ}$ versus 53.9 ± 0.4 µM in wild type, Fig. 3*F*).

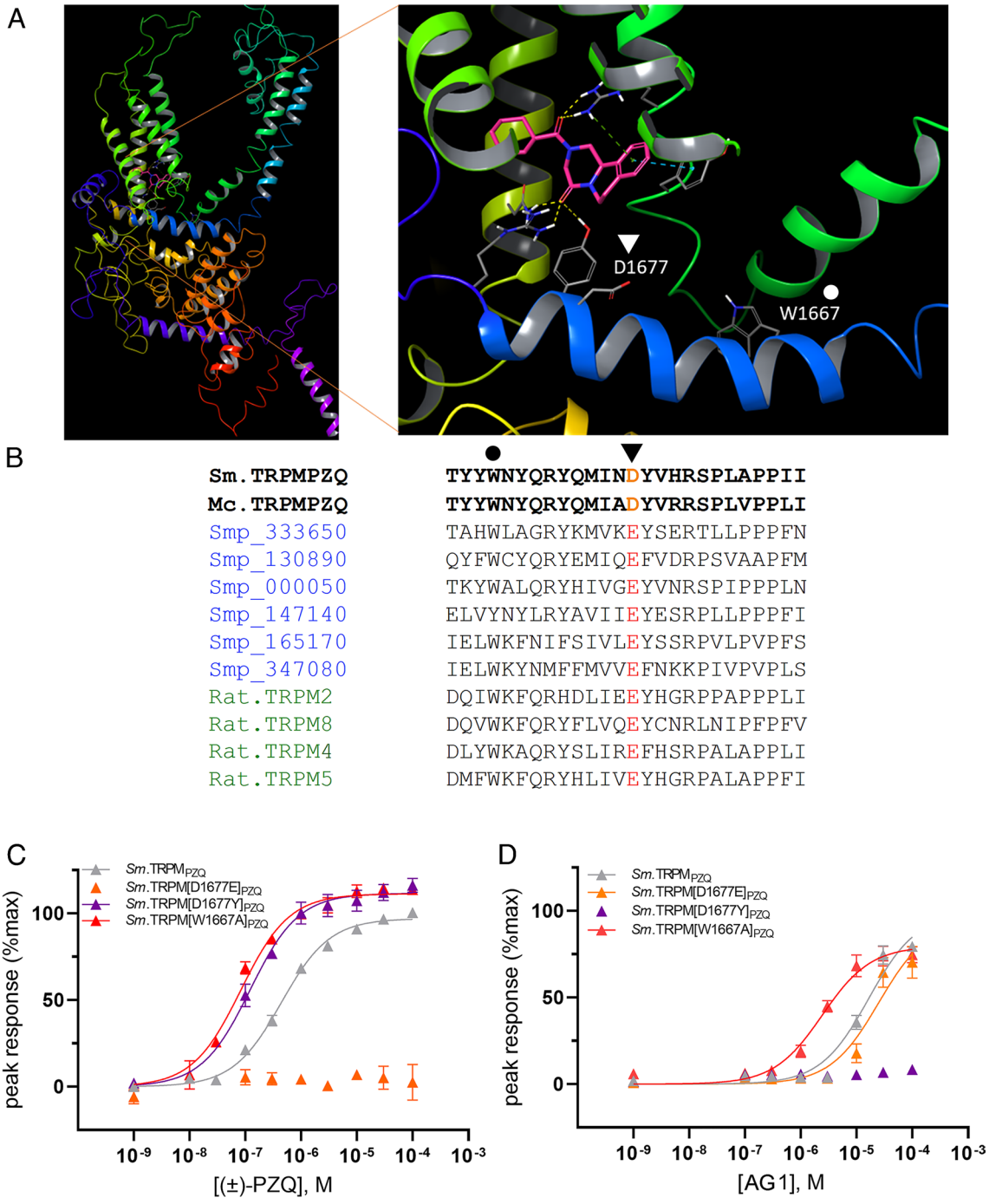

Fig. 4. Role of an acidic TRP helix residue as a gatekeeper regulating PZQ engagement within the VSLD binding pocket. (*A*) *Sm*.TRPM$_{PZQ}$ homology model (from (8)) with enlargement showing the binding pose of (*R*)-PZQ within the VSLD binding pocket in relation to TRP helix residues D1677 (triangle) and W1667 (circle). (*B*) Sequence alignment of a trematode TRPM$_{PZQ}$ (*Sm*.TRPM$_{PZQ}$) and cyclophyllidean cestode TRPM$_{PZQ}$ (*Mc*.TRPM$_{PZQ}$) highlighting the TRP domain aspartic acid residue (D1677, triangle) that is present in parasites that display the highest sensitivity to PZQ. Other predicted schistosome TRPM channels (gene identifiers in blue) and vertebrate Ca^{2+}-sensitive TRPM channels (green) possess a glutamic acid residue at the same position. A residue that regulates TRP channel gating (W1667) interrogated by mutagenesis in (*C*&*D*) is also highlighted (circle). (*C* and *D*) Differential effects of TRP helix mutants on ligand activation of *Sm*.TRPM$_{PZQ}$. Concentration–response curves for (*C*) (±)-PZQ and (*D*) AG1 activation of *Sm*.TRPM[D1677Y]$_{PZQ}$ (purple), *Sm*.TRPM[D1677E]$_{PZQ}$ (orange), and *Sm*.TRPM[W1667A]$_{PZQ}$ compared with wild-type *Sm*.TRPM$_{PZQ}$ (gray).

Collectively, these data highlight the importance of this variant acidic residue ('D' or 'E') found in the TRP helix as a key determinant of $TRPM_{PZQ}$ sensitivity toward PZQ (Fig. 4*A*). The aspartic acid variant was unique to trematode and cyclophyllidean cestode $TRPM_{PZQ}$, and these channels and these parasites exhibit the highest sensitivity to PZQ. The glutamic acid variant, associated with lower sensitivity to PZQ, was naturally present in monogeneans, pseudophyllidean cestodes, and free-living flatworm $TRPM_{PZQ}$ (*SI Appendix*, Table S2). This glutamic acid residue is also found in the TRP helix of all other schistosome TRPM family members (Fig. 4*B*), none of which have been reported to show sensitivity to PZQ (6). It is also present in the vertebrate TRPM channels TRPM2 and TRPM8 (which most closely resemble $TRPM_{PZQ}$ (7), Fig. 4*B*). Human TRPM8 responds to (*S*)-PZQ only in the micromolar range [EC_{50} for human TRPM8 to (*S*)-PZQ = ~20 μM (36, 37)].

How Does This Residue Impact PZQ Sensitivity?. This variant TRP helix residue (D1677) is situated just beneath the PZQ binding pocket mapped within the VSLD of $TRPM_{PZQ}$ (Fig. 4*A*). This would suggest that the identity of the acidic residue impacts ligand binding in the pocket. However, given that the TRP domain is important for transducing the binding of ligands into channel activation, an alternative possibility is that this variation impacts channel gating rather than ligand binding. If this were the case, then the 'D' to 'E' variation would have the same deleterious effect for different ligands. Assays performed with the two known activating ligands of *Sm*.$TRPM_{PZQ}$—PZQ and AG1 (38)—revealed that the effects of this residue on gating were not the explanation for the differential sensitivity to PZQ. While *Sm*.$TRPM[D1677E]_{PZQ}$ ablated sensitivity to PZQ, responses to AG1 were unaffected (Fig. 4 *C* and *D*). In contrast, a different mutant at this same position—*Sm*.$TRPM[D1677Y]_{PZQ}$—enhanced PZQ sensitivity but ablated AG1 responsiveness (Fig. 4*D*). Therefore, variation at this position confers differential effects on different ligands, implicating effects on ligand binding. In contrast, mutation of a tryptophan residue (W1667A, Fig. 4*A*) in the TRP helix that is positioned further away from the binding pocket and known to regulate channel gating (39, 40) caused increased sensitivity to both ligands (Fig. 4 *C* and *D*). Therefore, variation at D1677 impacts channel sensitivity to PZQ by altering PZQ engagement within the VSLD binding pocket.

To investigate how amino acid variation at residue 1677 impacted ligand binding, we utilized molecular dynamics (MD) to model residue flexibility and conformational changes at the atomic level. MD permits the appreciation of key ligand–receptor interactions and ligand stability within a binding pocket. For each of the TRP helix variants (wild type, D1677E, and D1677Y), seven independent MD simulations (500 ns duration) of the channel complexed with (*R*)-PZQ were simulated, compiling 3500 ns of data for each variant (70,000 total frames). Each trajectory was clustered to resolve the most likely binding pose from all those sampled during each run, and these poses were superimposed. For all three variants, (*R*)-PZQ occupied the VSLD of the channel (Fig. 5 *A*, *C*, and *E*).

In wild-type *Sm*.$TRPM_{PZQ}$, the (*R*)-PZQ binding poses clustered together and recapitulated critical ligand–protein interactions (Fig. 5*A* and ref. 8). For the D1677E variant, the clustered poses showed more variability (Fig. 5*C*). The top poses were displaced from the wild-type pose, and the interactions important for channel activation were absent (8). Poses from the *Sm*.$TRPM[D1677Y]_{PZQ}$ simulations clustered together but were deeper into the VSLD pocket (Fig. 5*E*), suggesting additional attractive interactions between the ligand and channel.

The root-mean-square deviation (RMSD) of the ligand during simulation was obtained from these MD trajectories as a measure of ligand stability in the binding pocket with respect to the modeled protein. Larger RMSD values indicated greater movement of the ligand from the reference binding pose, inversely correlating with the stability of the initial pose. For (*R*)-PZQ in the WT channel, the ligand was stable throughout these simulations (Fig. 5*B*): analysis of the RMSD across all 70,000 frames yielded a median RMSD of 2.9 Å (Fig. 5*G*). This contrasted with MD simulations of *Sm*.$TRPM[D1677E]_{PZQ}$, where (*R*)-PZQ displayed an increased RMSD, and in multiple runs, the ligand diffused away from the binding pocket. Fig. 5*D* shows the RMSD of the ligand immediately jumped to >5 Å and never returned to the baseline. Analysis of the RMSD of all 70,000 frames from the *Sm*.$TRPM[D1677E]_{PZQ}$ simulation yielded a median RMSD of 5.1 Å (Fig. 5*G*). This suggested that (*R*)-PZQ is less stable within the D1677E variant binding pocket compared to the WT channel. For *Sm*.$TRPM[D1677Y]_{PZQ}$, (*R*)-PZQ stabilized almost immediately in the VSLD pocket and remained in place throughout the simulation (Fig. 5*F*). Analysis of the RMSD of all 70,000 frames from this simulation revealed a median RMSD of 4.1 Å (Fig. 5*G*). The RMSD in this variant represented a shift of the ligand into a stabilized pose deeper within the binding pocket than seen with the WT channel. For each of the three variants, protein RMSD stabilized at ~9 Å across each individual run (green tracings, Fig. 5 *B*, *D*, *F*, and *H*), with analyses of all 70,000 frames suggesting similar protein flexibility for each variant. Overall, these unbiased MD simulations revealed that when starting from the ligand–channel pose containing the proposed critical residue interactions (8), (*R*)-PZQ remains stable in its binding orientation. The D1677E variant disrupted these interactions with (*R*)-PZQ exhibiting increased movement. The D1677Y variant captured (*R*)-PZQ deeper within the binding pocket.

To sample more of the conformational landscape of these ligand–channel complexes, we employed metadynamics as a second modeling approach (41, 42). Metadynamics facilitates extended sampling of ligand–receptor binding conformations, and this methodology has been used to reconstruct the full free-energy landscape of protein-ligand binding (41, 43, 44). With this approach, the lowest energy binding pose and corresponding ligand–channel interactions can be determined along a given collective variable (CV). When the wild-type complex was subjected to metadynamics, employing the distance between the center of mass of (*R*)-PZQ and the center of mass of D1677 as the CV, the lowest free-energy pose reproduced key interactions between (*R*)-PZQ and VSLD binding pocket residues (Fig. 6 *A* and *B*). (*R*)-PZQ was anchored in the pocket by hydrogen bonding and cation–π interactions with R1514 (S4) and a hydrogen bond with N1388 (S1). These interactions have previously shown to be important for engaging (*R*)-PZQ (8). However, D1677 formed a hydrogen bond with Q1673 one turn further along the TRP helix. This interaction pulled the D1677 side chain away from the VSLD binding pocket, precluding any interference with (*R*)-PZQ association.

The lowest free-energy pose for (*R*)-PZQ in *Sm*.$TRPM[D1677E]_{PZQ}$ was distinctly different from the lowest free-energy pose of (*R*)-PZQ in the wild-type channel. Metadynamics revealed two energy minima—a relative minimum ('metastable state') and an absolute minimum (Fig. 6*C*). In the pose associated with the relative minimum, the side chain of the variant glutamate residue projects into the VSLD binding pocket, resulting in (*R*)-PZQ displacement (*SI Appendix*, Fig. S2) In the pose associated with the absolute minimum, (*R*)-PZQ was also completely displaced from any binding pocket interactions, with E1677 projected into the binding pocket (Fig. 6*D*). The observed lower free energy resulted from new stabilizing hydrogen bond interactions that formed within

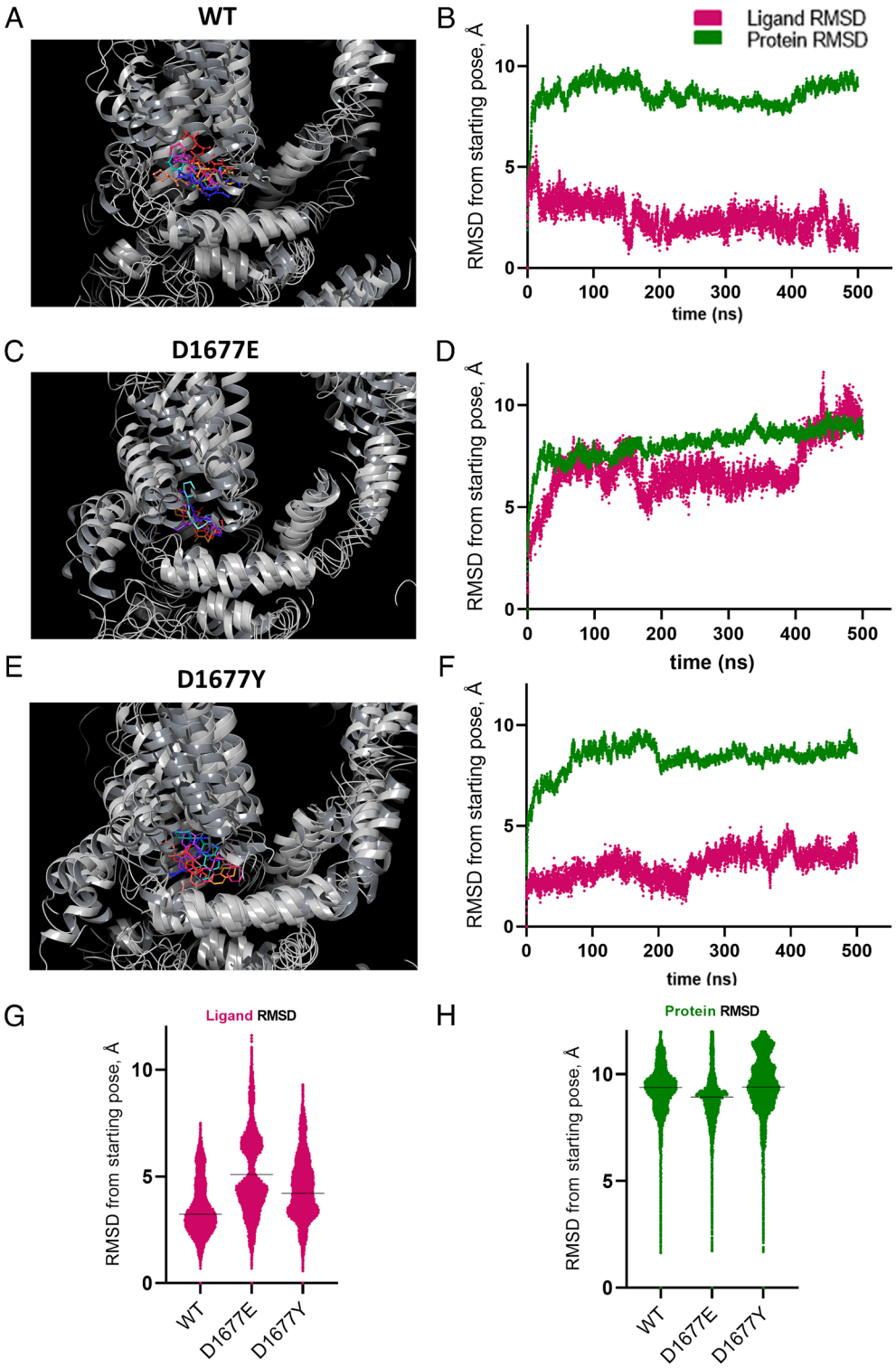

Fig. 5. MD Simulations of (*R*)-PZQ complexed with *Sm*.TRPM$_{PZQ}$ TRP helix variants. (*A*) Superposition of the top pose from each of seven independent 500 ns MD runs of (*R*)-PZQ in complex with WT *Sm*.TRPM$_{PZQ}$. The channel is depicted in gray, (*R*)-PZQ is colored. (*B*) Representative RMSD trace of a single 500-ns trajectory (10,000 frames) of (*R*)-PZQ complexed with wild-type *Sm*.TRPM$_{PZQ}$ with both ligand RMSD (maroon) and protein RMSD (green) represented. RMSD is measured in reference to the C_α of the channel. (*C* and *D*) As in *A* and *B* but with *Sm*.TRPM[D1677E]$_{PZQ}$. (*E* and *F*) As in *A* and *B* but with *Sm*.TRPM[D1677Y]$_{PZQ}$. (*G*) Plot of ligand RMSD of all combined 70,000 frames of MD simulation for each TRP helix variant referenced to the C_α of the channel. The black line indicates the median RMSD of the cumulative 3,500 ns of simulation (WT = 2.9 Å, D1677E = 5.1 Å, D1677Y = 4.1 Å). (*H*) Plot of the protein RMSD of all combined 70,000 frames of MD simulation for each TRP helix variant referenced to the C_α of the channel. The black line indicates the median RMSD of the cumulative 3500 ns of simulation (WT = 9.3 Å, D1677E = 8.9 Å, D1677Y = 9.4 Å).

the pocket: E1677 with R1514 and W1451 (Fig. 6*D*). These new hydrogen bonding interactions prevent (*R*)-PZQ interaction with R1514, an interaction critical for (*R*)-PZQ-evoked channel activation (8). The *Sm*.TRPM[D1677Y]$_{PZQ}$ complex with (*R*)-PZQ was also subjected to metadynamics. In the lowest free-energy pose, (*R*)-PZQ acquired new π–π stacking interactions with the phenol of Y1677 (Fig. 6 *E* and *F*) and was anchored in place through the hydrogen bond interaction with R1514. This prediction of a new

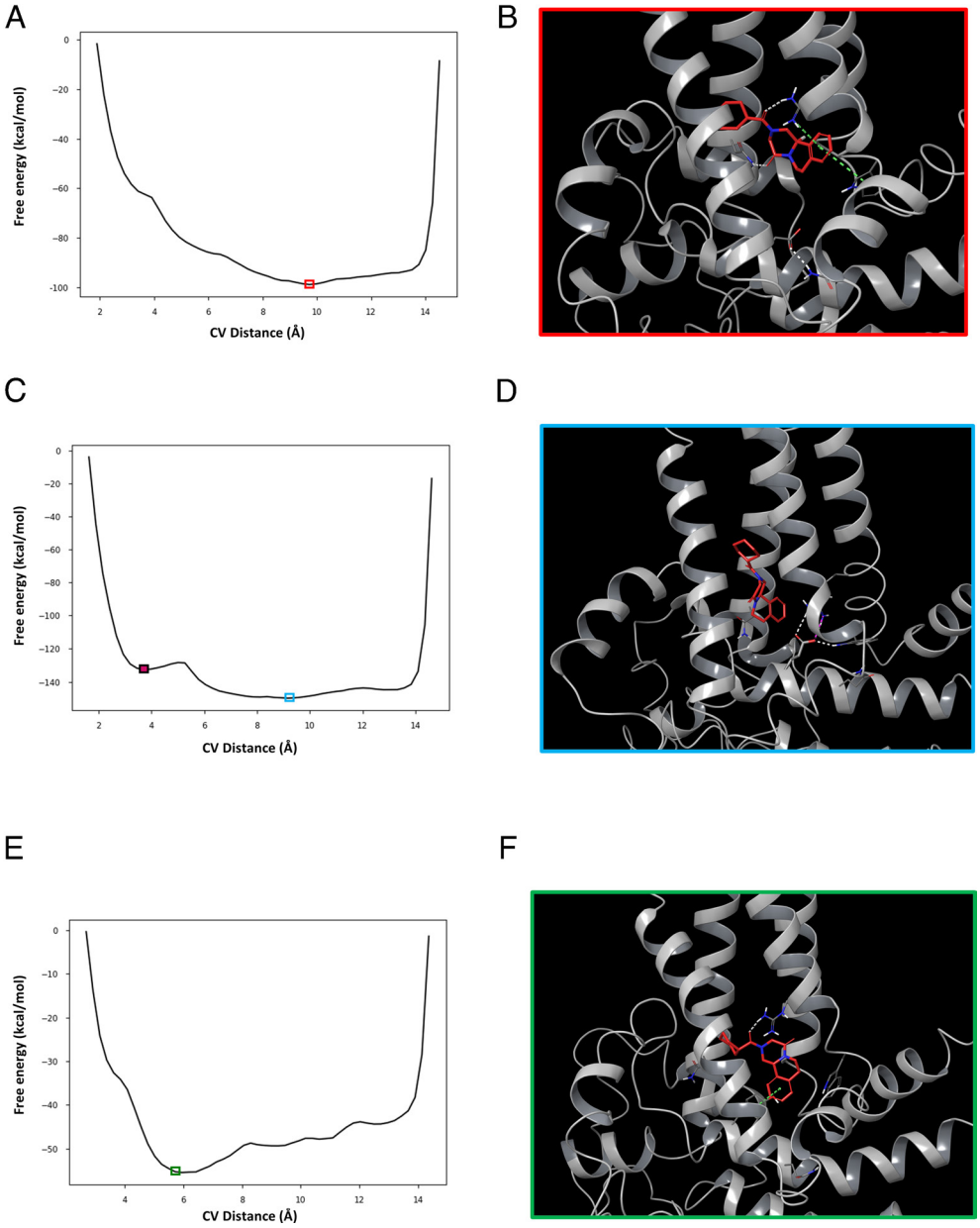

Fig. 6. Metadynamics simulations of (*R*)-PZQ complexed with *Sm*.TRPM$_{PZQ}$ TRP helix variants. (*A*) Representative free-energy plot resulting from metadynamics simulations of (*R*)-PZQ complexed with wild-type *Sm*.TRPM$_{PZQ}$. The x-axis is the CV, set as the distance between the center of mass of (*R*)-PZQ and the center of mass of D1677 (in Å). The y-axis shows the free energy of that interaction (in kcal/mol). The red box encloses the lowest energy frame from the simulation. (*B*) The binding pose of (*R*)-PZQ within *Sm*.TRPM$_{PZQ}$ from the lowest energy frame from panel *A*. (*R*)-PZQ forms hydrogen bonds (dashed white lines) with R1514 and N1388, cation–π interactions with R1514, and π–π stacking interactions with W1451 (dashed green lines). D1677 is pulled away from the pocket *via* a hydrogen bond with Q1673. (*C*) Representative free-energy plot resulting from metadynamics simulations of (*R*)-PZQ complexed with *Sm*.TRPM[D1677E]$_{PZQ}$ as in *A*. The solid maroon box encloses the frame representing the relative minima of the simulation (pose shown in *SI Appendix*, Fig. S2). The blue box encloses the lowest energy frame from the simulation. (*D*) The binding pose of (*R*)-PZQ within *Sm*.TRPM[D1677E]$_{PZQ}$ in the lowest energy frame from the simulation. (*R*)-PZQ is displaced from any binding interactions and E1677 points into the binding pocket, forming hydrogen bonds (dashed white lines) and a salt bridge with R1514 (dashed magenta line) and a hydrogen bond with W1451. (*E*) Representative free-energy plot from metadynamics simulations of (*R*)-PZQ complexed with *Sm*.TRPM[D1677Y]$_{PZQ}$ as in *A*. The green box encloses the lowest energy frame from the simulation. (*F*) The binding pose of (*R*)-PZQ within *Sm*.TRPM[D1677Y]$_{PZQ}$ in the lowest energy frame from the simulation. (*R*)-PZQ binds within the VSLD of the channel, forming a hydrogen bond (dashed white line) with R1514 and π–π stacking (dashed green line) with Y1677.

interaction with PZQ was consistent with the increased potency of PZQ in functional assays (Fig. 4*C*). A comparison of the (*R*)-PZQ binding pose in *Sm*.TRPM$_{PZQ}$ and *Sm*.TRPM[D1677E]$_{PZQ}$ with the binding pose adopted by TRPM8 ligands within *Hs*.TRPM8 (45, 46) is shown in *SI Appendix*, Fig. S3.

Therefore, both MD analyses (Fig. 5) and metadynamics (Fig. 6) demonstrated that the TRP helix aspartate to glutamate variation in *Sm*.TRPM$_{PZQ}$ displaced (*R*)-PZQ from productive interactions within the VSLD binding pocket, consistent with the decreased PZQ sensitivity of parasitic flatworm TRPM$_{PZQ}$ channels containing this variation.

Discussion

In this study, we have profiled the PZQ binding pocket of TRPM$_{PZQ}$ orthologs in all currently available parasitic flatworm genomes: TRPM$_{PZQ}$ is present in all parasitic flatworms examined, and the PZQ binding site is well conserved. In trematodes, functional

profiling of six $TRPM_{PZQ}$ orthologs demonstrated stereoselective activation by (*R*)-PZQ in the submicromolar range (EC_{50} for (*R*)-PZQ = ~90 to 320 nM, Figs. 1 and 2). These include $TRPM_{PZQ}$ from the three species of schistosomes (*S. mansoni*, *S. haematobium,* and *S. japonicum*) responsible for the majority of infections worldwide, as well as $TRPM_{PZQ}$ from *E. caproni*, *C. sinensis*, and *O. viverrini*. In all these $TRPM_{PZQ}$ orthologs, the key PZQ binding pocket residues are identical (Fig. 2*A* and *SI Appendix*, Table S2), and PZQ sensitivity of this TRP channel is consistent with the known PZQ sensitivity of these parasites in vitro and in vivo. We predict the consensus $TRPM_{PZQ}$ pocketome will also be conserved in other trematodes where $TRPM_{PZQ}$ sequence information is currently lacking (1, 25, 31, 47–49), given the known efficacy of PZQ for treating other diseases caused by these parasites. The only exception found was the identification of a single amino acid variant within the $TRPM_{PZQ}$ pocket of *Fasciola spp*. (*F. hepatica* and *F. gigantica*). *Fh*.$TRPM_{PZQ}$ and *Fg*.$TRPM_{PZQ}$ were refractory to PZQ, consistent with the lack of PZQ efficacy in treating infections caused by these liver flukes (10). However, both *Fasciola spp.* $TRPM_{PZQ}$ channels gained PZQ sensitivity when the S1 variant threonine was substituted for an asparagine residue to mimic the trematode consensus sequence (Fig. 2*F* and ref. 8). It will be of interest to further analyze the *Fasciolidae* to understand the evolution of this pocket between closely related liver flukes (50) and determine if this S1 residue variation is specific to just the *Fasciola* genus. Key representatives for analysis would be from the genera *Fascioloides* (e.g., *F. magna), Protofasciola,* and *Parafasciolopsis*.

While *Fasciola* provide a stark example showing how differential species sensitivity to a TRP channel ligand has impact on disease treatment, the principle that TRP channel sequence variation imparts species-specific ligand sensitivity has been previously recognized. Differences between avian and mammalian TRPV1 sequences underpin the tolerance of birds to capsaicin, an adaptation thought to aid seed dispersal (51, 52). Variation of an S4 residue in tree shrew TRPV1 confers insensitivity to an analog of capsaicin, so that this particular species of tree shrew is indifferent to the consumption of spicy plants (53). This specific variant is predicted to remove a critical hydrogen bonding interaction with the ligand (53), paralleling the effect of sequence variation at a key hydrogen-binding position in the S1 helix of $TRPM_{PZQ}$ underlying the insensitivity of *Fasciola spp*. $TRPM_{PZQ}$ to PZQ (8). Possibly, this binding pocket variation within *Fasciola spp*. $TRPM_{PZQ}$ holds significance for (dis)engagement of natural products or metabolites that are uniquely encountered during the *Fasciola* lifecycle.

PZQ is also effective for combating other parasitic flatworm infections (1, 5, 10–12). PZQ is highly effective against cyclophyllidean cestodes (1, 54–57), with deleterious effects occurring at very low PZQ concentrations in vitro [as low as 320 pM, (55)]. This is consistent with functional analyses of *E. granulosus* $TRPM_{PZQ}$ (*Eg*.$TRPM_{PZQ}$) and *M. corti* $TRPM_{PZQ}$ (*Mc*.$TRPM_{PZQ}$) which both displayed extremely high sensitivity to PZQ. This sensitivity occurred despite differences between these tapeworm ('HSD' configuration) and trematode ('NTD') $TRPM_{PZQ}$ binding pockets (Fig. 3*B*). Interestingly, the structure–activity relationships of PZQ analogs against trematodes and cestodes are different (1) such that these variant residues (Fig. 3*B*) likely contribute to the ability of trematode and cestode $TRPM_{PZQ}$ to accommodate different ligands.

For all other flatworms, the presence of the glutamic acid TRP domain residue (Fig. 4*A*) is important as this variant confers lower sensitivity to PZQ (*supra*micromolar rather than *sub*micromolar). This holds clinical relevance as pseudophyllidean cestode species harboring this residue can cause a rare, but potentially serious, disease in humans (58, 59). There is prior evidence that pseudophyllidean tapeworms exhibit lower sensitivity to PZQ (15); for example, larval and adult diphyllobothriids required PZQ concentrations in excess of 320 μM to show lethality (60). This glutamic acid residue is also present in all monogeneans; the effective treatment of which is a priority for the aquaculture industry (12, 61). In polyopisthocotylean monogeneans, this glutamic acid variant occurs as the sole change from the trematode $TRPM_{PZQ}$ binding pocket consensus ('NTE' in *Protopolystoma xenopodis*) compared to monopisthocotylean monogeneans ('HTE' configuration in *Gyrodactylus spp*.) where the more accommodating S1 histidine variant is present. Differential sensitivities of monogenean species have been reported (12, 61), with evidence that polyopisthocotylean species require higher PZQ concentrations to manifest deleterious effects (62, 63). Similarly, the biological efficacy of PZQ against free-living flatworms, which also harbor the glutamic acid TRP domain residue, is in the micromolar range (EC_{50} = 35 ± 7 μM for PZQ evoking bipolarity in *D. japonica* (16)). Such lower sensitivity was supported here by functional analysis of *M. lignano* $TRPM_{PZQ}$ ('NIE' configuration) which was activated by micromolar (±)-PZQ concentrations (Fig. 3*F*). This molecular insight provides pause should this TRP domain variant (E1677 in *S. mansoni*, E1588 in *S. japonicum*, and E1605 in *S. haematobium*), which has evolved naturally in several flatworm lineages, were to be found in schistosome populations, for example, occurring in response to selection pressure evoked by mass drug administrative campaigns. Any decrease in the effectiveness of PZQ as a cheap, effective drug for treating schistosomiasis would be a significant public health challenge.

Mechanistically, the application of MD (Fig. 5) and metadynamics (Fig. 6) to simulate PZQ engagement within the wild-type *Sm*.$TRPM_{PZQ}$ and *Sm*.$TRPM[D1677E]_{PZQ}$ binding pocket confirmed the deleterious impact of the glutamic acid variant. The glutamic acid residue (E1677) projected into the VSLD, rather than along the TRP helix as occurred with the wild-type aspartic acid residue (D1677) which was anchored away from the binding pocket via an interaction with Q1673 (Fig. 6). The internal projection of E1677 within the VSLD positioned negative charge in too close proximity to the preferred (*R*)-PZQ binding pose or removed a key interaction for (*R*)-PZQ engagement as E1677 formed a hydrogen bond with R1514. These outcomes were represented as discrete energy minima in the metadynamics simulations (Fig. 6). Therefore, the identity of this TRP domain gatekeeper residue provides an answer to why infections with parasites carrying a glutamate at this position (monogeneans, pseudophyllidean cestodes) are clinically less sensitive to treatment with PZQ, while infections with parasites carrying an aspartate at this position (most trematodes and cyclophyllidean cestodes) uniquely display a high sensitivity to PZQ. This provides an opportunity to design better ligands tailored for the $TRPM_{PZQ}$ orthologs displaying lower sensitivity toward PZQ. Different ligands utilize different poses to engage the VSLD binding pocket, such that alternative chemotypes (for example, AG1 (38)) may better tolerate the glutamic acid TRP helix variant that impairs PZQ engagement (Fig. 4*D*).

In conclusion, the presence of $TRPM_{PZQ}$ in all parasitic flatworms sensitive to PZQ, and the correlation between $TRPM_{PZQ}$ sensitivity to PZQ and worm sensitivity to PZQ provides further support for $TRPM_{PZQ}$ acting as the relevant in vivo target of PZQ. The definition of the $TRPM_{PZQ}$ pocketome revealed the unique presence of an aspartic acid ('D') residue within the TRP helix of $TRPM_{PZQ}$ is critical for conferring high sensitivity to PZQ, and this underpins the unique efficacy of PZQ against trematode and cestode infections first observed over four decades ago (1).

Materials and Methods

Materials and Reagents. (±)-PZQ was purchased from Sigma, and the individual enantiomers (*R*)-PZQ and (*S*)-PZQ were resolved following published protocols (64). HEK-293 cell lines were sourced from ATCC (CRL-1573) and found to be negative for

mycoplasma contamination by monthly scheduled testing (LookOut® Mycoplasma PCR Detection Kit, Sigma). All cell culture reagents were from Invitrogen. Total RNA from adult male and female *S. haematobium* (Egyptian Strain, NR-31801) was provided by the NIAID Schistosomiasis Resource Center for distribution through BEI Resources, NIAID, NIH. Biological samples of different parasites were generously provided from various sources: *F. hepatica* (Paul McCusker, Maule lab, Queen's University, Belfast), *Gyrodactylus spp.* (Eric Leis, La Crosse Fish Health Center, US Fish and Wildlife Service), *M. corti* (Arun Chauhan, Mishra lab, University of North Dakota), *H. diminuta* (Elise Nanista, Rozario lab, University of Georgia), and *M. lignano* (Lisa Glazenburg, Berezikov lab, University of Groningen).

Bioinformatic Analyses. Genome sequences were accessed either through WormBase ParaSite v16 (33) or individual project data repositories deposited on NCBI. $TRPM_{PZQ}$ candidate sequences were identified by BLAST searches, and then genome sequence information was manually curated. For the calculation of $TRPM_{PZQ}$ amino acid identity, sequences were aligned using MAFFT (v6.864) and aligned sequences analyzed using the Ident and Sim interface using standard groups for amino acid similarity (65). The full-length sequence of *S. haematobium* $TRPM_{PZQ}$ (*Sh*.$TRPM_{PZQ}$) was cloned from *S. haematobium* total RNA using RT-PCR and 5'-RACE. 5′-RACE was performed using the SMARTer RACE 5′3′ Kit (Clontech). Briefly, total RNA (0.5 to 1 μg) was reverse-transcribed using a SMARTer II A Oligonucleotide (42 °C for 1.5 h) to obtain first-strand cDNA. 5′RACE RT-PCR was performed using first-strand cDNA, *Sh*.$TRPM_{PZQ}$ gene-specific primers, and a universal primer mix using the following touchdown PCR conditions: 5 cycles (94 °C for 30 s and 70 °C for 3 min), 5 cycles (94 °C for 30 s, 68 °C for 30 s, and 72 °C for 3 min), and then, the mixture was amplified for 30 cycles (94 °C for 30 s; 63 °C for 30 s and 72 °C for 3 min). The RACE PCR products were cloned into pRACE vector using In-Fusion Cloning system (Clontech) and sequenced (Retrogen, Inc).

FLIPR Ca $^{2+}$ Assay. The Fluorescence Imaging Plate Reader (FLIPR) Ca^{2+} reporter assay was performed in black-walled, clear-bottomed 384-well plates coated with poly-D-lysine (Greiner Bio-One, Germany). Briefly, nontransfected or transfected HEK293 cells were seeded (20,000 cells/well) in DMEM growth media containing 10% FBS. After 24 h, the medium was removed and replaced with 20 μL of Fluo-4 NW dye loading solution (Molecular Devices), previously reconstituted in assay buffer (Hanks' balanced salt solution with Ca^{2+}, Mg^{2+}, 20 mM HEPES, and 2.5 mM probenecid). Cells were incubated for 30 min at 37 °C (5% CO_2) followed by an additional 30-min incubation at room temperature. Drug dilutions were prepared in an assay buffer, but without probenecid and fluorescent dye, in 384-well plates (Greiner Bio-One). Using a $FLIPR^{TETRA}$ (Molecular Devices), basal fluorescence (filter settings λ_{ex} = 470 to 495 nm, λ_{em} = 515 to 575 nm) from each well was monitored for 20 s, then 5 μL of drug or vehicle solution was added (25 μL total volume) and the signal was recorded over 250 s. Changes in fluorescence were represented as relative fluorescence units after subtracting the average basal fluorescence (average basal fluorescence over 20 s) from the recorded values. Concentration–response analysis was performed using sigmoidal curve fitting functions in Prism using data from n ≥ 3 independent transfections, with n ≥ 3 technical replicates per assay.

Computational Procedures. Generation of the *Sm*.$TRPM_{PZQ}$ homology model has been previously described (8). *Sm*.$TRPM[D1677E]_{PZQ}$ and *Sm*.$TRPM[D1677Y]_{PZQ}$ homology models were created by making the desired mutant of the Sm.$TRPM_{PZQ}$ wild-type homology model in the Schrodinger Computational Suite (v2022-1) followed by minimization of the protein using the Protein Preparation Wizard in the OPLS4 force field at pH = 7.4 (66). To prepare ligands for modeling, (*R*)-PZQ was drawn in ChemDraw Professional (v21.0.0), imported into the Maestro GUI (*v.* 13.1), and prepared using the LigPrep tool with default settings in the OPLS4 force field at pH = 7.4. The output structure was used for subsequent modeling.

MD simulations. Unbiased MD were performed using Desmond within the Schrodinger Computational Suite (67). For *Sm*.$TRPM_{PZQ}$, the protein–ligand complex was inserted into a POPC membrane bilayer using the 'System Builder', aligning the membrane coordinates to PDB 6NR3 in the OPM database. Solvation was treated explicitly using the SPC water model with 0.15 M NaCl, charges were neutralized by adding Na^+ or Cl^- ions when necessary, and the membrane was generated in the OPLS4 force field. The system was minimized to a protein RMSD <0.3 Å, and the minimized system was used as the starting pose for MD simulations. Seven independent runs of 500 ns were completed. The simulations were run in the NPγT ensemble using both the Langevin thermostat (300 K) and semiisotropic barostat (1.01325 bar). The system was relaxed before simulation and gradually brought to temperature with decreasing constraints as per the default series of Desmond simulations. Each simulation began from a random seed, the velocities were randomized, and frames were recorded at an interval of 50 ps which allowed for the collection of 10,000 frames in each simulation. *Sm*.$TRPM[D1677E]_{PZQ}$ and *Sm*.$TRPM[D1677Y]_{PZQ}$ were prepared, and simulations were executed in an identical manner. Each of the seven runs for each channel variant was independently clustered using the 'Trajectory Clustering Tool' within the Maestro GUI. The poses of the most populated cluster from each run were then superimposed as depicted in Fig. 5. Ligand and protein RMSD–the average change in displacement of selected atoms for a particular MD frame with respect to a reference frame–were calculated from MD simulations with reference to the Cα of the protein in the input structure using the Maestro GUI of the Schrodinger Computational Suite. Images were plotted, and median calculations were performed, using GraphPad Prism (v9.3.1).

Metadynamics. The minimized, solvated systems for metadynamics simulations were generated as described for the MD Simulations and then run using Desmond (67). The CV was set as the distance between the center of mass of (*R*)-PZQ and the center of mass of the side chain of residue 1677 (D1677 for WT *Sm*.$TRPM_{PZQ}$, E1677 for *Sm*.$TRPM[D1677E]_{PZQ}$, and Y1677 for *Sm*.$TRPM[D1677Y]_{PZQ}$). The Gaussian width and height were set at 0.025 Å and 0.015 kcal/mol, respectively, and deposited at 0.09 ps intervals, and a necessary wall was placed at 15 Å to keep the ligand in the VSLD of the channel. Simulations were run in the NPγT ensemble using the Langevin thermostat (300 K) and Langevin barostat (1.01325 bar). Independent simulations of 50 ns were run for each channel variant, starting from a random seed number and randomizing atom velocities for each simulation. Using the 'metadynamics analysis' tool in Maestro, free energy of the system (ΔG) was plotted versus the CV (Å) to produce a free-energy diagram corresponding to every frame in the metadynamics simulation, as presented in Fig. 6.

Data, Materials, and Software Availability. All study data are included in the article and/or *SI Appendix*.

ACKNOWLEDGMENTS. This research in the Marchant lab was supported by the National Institutes of Health (R01-AI145871 to J.S.M.). N.J.M. was supported from T32 GM080202 (Medical Scientist Training Program). D.J.S. acknowledges the support from the NIH (T32 HL134643) and the MCW Cardiovascular Center's A.O. Smith Fellowship Scholars Program. We acknowledge the computational resources and technical support provided by the Research Computing Center at the Medical College of Wisconsin.

Author affiliations: [a]Department of Cell Biology, Neurobiology and Anatomy, Medical College of Wisconsin, Milwaukee, WI 53226

1. P. Andrews, H. Thomas, R. Pohlke, J. Seubert, Praziquantel. *Med. Res. Rev.* **3**, 147–200 (1983).
2. D. G. Colley, A. L. Bustinduy, W. E. Secor, C. H. King, Human schistosomiasis. *Lancet* **383**, 2253–2264 (2014).
3. D. P. McManus *et al.*, Schistosomiasis. *Nat. Rev. Dis. Primers* **4**, 13 (2018).
4. H. Mehlhorn *et al.*, In vivo and in vitro experiments on the effects of praziquantel on *Schistosoma mansoni*. A light and electron microscopic study. *Arzneimittelforschung.* **31**, 544–554 (1981).
5. R. Gonnert, P. Andrews, Praziquantel, a new board-spectrum antischistosomal agent. *Z. Parasitenkd.* **52**, 129–150 (1977).
6. S. K. Park *et al.*, The anthelmintic drug praziquantel activates a schistosome transient receptor potential channel. *J. Biol. Chem.* **294**, 18873–18880 (2019).
7. S. K. Park, J. S. Marchant, The journey to discovering a flatworm target of praziquantel: A long TRP. *Trends Parasitol.* **36**, 182–194 (2020).
8. S. K. Park *et al.*, Mechanism of praziquantel action at a parasitic flatworm ion channel. *Sci. Transl. Med.* **13**, eabj5832 (2021).
9. W. Le Clec'h *et al.*, Genetic analysis of praziquantel response in schistosome parasites implicates a transient receptor potential channel. *Sci. Transl. Med.* **13**, eabj9114 (2021).
10. J. Y. Chai, Praziquantel treatment in trematode and cestode infections: An update. *Infect. Chemother.* **45**, 32–43 (2013).
11. H. Thomas, R. Gonnert, The efficacy of praziquantel against cestodes in animals. *Z. Parasitenkd.* **52**, 117–127 (1977).

12. C. Bader, D. E. Starling, D. E. Jones, M. T. Brewer, Use of praziquantel to control platyhelminth parasites of fish. *J. Vet. Pharmacol. Ther.* **42**, 139–153 (2019).
13. L. Mikes *et al.*, In vitro stimulation of penetration gland emptying by *Trichobilharzia szidati* and *T. regenti* (Schistosomatidae) cercariae. Quantitative collection and partial characterization of the products. *Parasitol. Res.* **96**, 230–241 (2005).
14. N. Hirazawa, K. Akiyama, N. Umeda, Differences in sensitivity to the anthelmintic praziquantel by the skin-parasitic monogeneans *Benedenia seriolae* and *Neobenedenia girellae*. *Aquaculture* **404**, 59–64 (2013).
15. M. A. Gemmell, P. D. Johnstone, Cestodes. *Antibiot. Chemother.* **1971**, 54–114 (1981).
16. T. Nogi, D. Zhang, J. D. Chan, J. S. Marchant, A novel biological activity of praziquantel requiring voltage-operated Ca2+ channel beta subunits: subversion of flatworm regenerative polarity. *PLoS Negl. Trop. Dis.* **3**, e464 (2009).
17. D. Zhang, J. D. Chan, T. Nogi, J. S. Marchant, Opposing roles of voltage-gated Ca^{2+} channels in neuronal control of stem cell differentiation *in vivo*. *J. Neurosci.* **31**, 15983–15995 (2011).
18. G. H. Horan, "The microturbellarian *Macrostomum ligano* as a model for the study of parasitic worms", PhD thesis, Queen's University, Belfast, United Kingdom (2014).
19. K. Cwiklinski, S. M. O'Neill, S. Donnelly, J. P. Dalton, A prospective view of animal and human Fasciolosis. *Parasite Immunol.* **38**, 558–568 (2016).
20. D. P. McManus, Recent progress in the development of liver fluke and blood fluke vaccines. *Vaccines (Basel)* **8**, 553 (2020).
21. I. Meister *et al.*, Activity of praziquantel enantiomers and main metabolites against *Schistosoma mansoni*. *Antimicrob. Agents Chemother.* **58**, 5466–5472 (2014).
22. P. Horak *et al.*, Avian schistosomes and outbreaks of cercarial dermatitis. *Clin. Microbiol. Rev.* **28**, 165–190 (2015).
23. J. Monrad *et al.*, Treatment efficacy and regulatory host responses in chronic experimental *Schistosoma bovis* infections in goats. *Parasitology* **133**, 151–158 (2006).
24. D. M. de Vienne, Lifemap: Exploring the entire tree of life. *PLoS Biol* **14**, e2001624 (2016).
25. H. Mehlhorn *et al.*, Ultrastructural investigations on the effects of praziquantel on human trematodes from Asia: Clonorchis sinensis, *Metagonimus yokogawai*, *Opisthorchis viverrini*, *Paragonimus westermani* and *Schistosoma japonicum*. *Arzneimittelforschung* **33**, 91–98 (1983).
26. S. H. Lee *et al.*, *In vitro* effect of praziquantel on *Paragonimus westermani* by light and scanning electron microscopic observation. *Kisaengchunghak Chapchi.* **25**, 24–36 (1987).
27. B. Becker *et al.*, Light and electron microscopic studies on the effect of praziquantel on *Schistosoma mansoni*, *Dicrocoelium dendriticum*, and *Fasciola hepatica* (Trematoda) *in vitro*. *Z. Parasitenkd.* **63**, 113–128 (1980).
28. A. M. Dadak, C. Wieser, A. Joachim, S. Franz, Efficacy and safety of oral praziquantel against *Dicrocoelium dendriticum* in llamas. *Vet. Parasitol.* **197**, 122–125 (2013).
29. R. J. Johnson *et al.*, Paragonimiasis: diagnosis and the use of praziquantel in treatment. *Rev. Infect. Dis.* **7**, 200–206 (1985).
30. T. Harinasuta, D. Bunnag, P. Radomyos, Efficacy of praziquantel on fasciolopsiasis. *Arzneimittelforschung.* **34**, 1214–1215 (1984).
31. H. Taraschewski *et al.*, Effects of praziquantel on human intestinal flukes (*Fasciolopsis buski* and *Heterophyes heterophyes*). *Zentralbl. Bakteriol. Mikrobiol. Hyg. A* **262**, 542–550 (1986).
32. W. M. Arafa, K. M. Shokeir, A. M. Khateib, Comparing an in vivo egg reduction test and in vitro egg hatching assay for different anthelmintics against Fasciola species, in cattle. *Vet. Parasitol.* **214**, 152–158 (2015).
33. K. L. Howe *et al.*, WormBase ParaSite - a comprehensive resource for helminth genomics. *Mol. Biochem. Parasitol.* **215**, 2–10 (2017).
34. D. L. Morris, K. S. Richards, J. B. Chinnery, Protoscolicidal effect of praziquantel–in-vitro and electron microscopical studies on *Echinococcus granulosus*. *J. Antimicrob. Chemother.* **18**, 687–691 (1986).
35. M. M. Markoski *et al.*, Praziquantel and albendazole damaging action on in vitro developing *Mesocestoides corti* (Platyhelminthes: Cestoda). *Parasitol. Int.* **55**, 51–61 (2006).
36. G. S. Gunaratne, N. A. Yahya, P. I. Dosa, J. S. Marchant, Activation of host transient receptor potential (TRP) channels by praziquantel stereoisomers. *PLoS Negl. Trop. Dis.* **12**, e0006420 (2018).
37. R. M. Babes, T. Selescu, D. Domocos, A. Babes, The anthelminthic drug praziquantel is a selective agonist of the sensory transient receptor potential melastatin type 8 channel. *Toxicol. Appl. Pharmacol.* **336**, 55–65 (2017).
38. E. G. Chulkov *et al.*, Identification of novel modulators of a schistosome transient receptor potential channel targeted by praziquantel. *PLoS Negl. Trop. Dis.* **15**, e0009898 (2021).
39. Y. Huang *et al.*, Architecture of the TRPM2 channel and its activation mechanism by ADP-ribose and calcium. *Nature* **562**, 145–149 (2018).
40. J. Teng, S. H. Loukin, A. Anishkin, C. Kung, A competing hydrophobic tug on L596 to the membrane core unlatches S4–S5 linker elbow from TRP helix and allows TRPV4 channel to open. *Proc. Natl. Acad. Sci. U.S.A.* **113**, 11847–11852 (2016).
41. A. Laio, M. Parrinello, Escaping free-energy minima. *Proc. Natl. Acad. Sci. U.S.A.* **99**, 12562–12566 (2002).
42. V. Leone, F. Marinelli, P. Carloni, M. Parrinello, Targeting biomolecular flexibility with metadynamics. *Curr. Opin. Struct. Biol.* **20**, 148–154 (2010).
43. M. Incerti *et al.*, Metadynamics for perspective drug design: Computationally driven synthesis of new protein-protein interaction inhibitors targeting the EphA2 receptor. *J. Med. Chem.* **60**, 787–796 (2017).
44. F. L. Gervasio, A. Laio, M. Parrinello, Flexible docking in solution using metadynamics. *J. Am. Chem. Soc.* **127**, 2600–2607 (2005).
45. Y. Yin *et al.*, Structural basis of cooling agent and lipid sensing by the cold-activated TRPM8 channel. *Science* **363**, eaav9334 (2019).
46. Y. Yin *et al.*, Activation mechanism of the mouse cold-sensing TRPM8 channel by cooling agonist and PIP2. *Science* **378**, eadd1268 (2022).
47. J. Y. Chai, E. H. Shin, S. H. Lee, H. J. Rim, Foodborne intestinal flukes in Southeast Asia. *Korean J. Parasitol.* **47**, S69–102 (2009).
48. S. H. Lee, In vitro effects of praziquantel on *Fibricola seoulensis*. *Seoul J. Med.* **26**, 41–51 (1985).
49. W. J. Foreyt, J. R. Gorham, Evaluation of praziquantel against induced *Nanophyetus salmincola* infections in coyotes and dogs. *Am. J. Vet. Res.* **49**, 563–565 (1988).
50. Y. J. Choi *et al.*, Adaptive radiation of the flukes of the family fasciolidae inferred from genome-wide comparisons of key species. *Mol. Biol. Evol.* **37**, 84–99 (2020).
51. S. E. Jordt, D. Julius, Molecular basis for species-specific sensitivity to "hot" chili peppers. *Cell* **108**, 421–430 (2002).
52. Y. Chu, B. E. Cohen, H. H. Chuang, A single TRPV1 amino acid controls species sensitivity to capsaicin. *Sci. Rep.* **10**, 8038 (2020).
53. Y. Han *et al.*, Molecular mechanism of the tree shrew's insensitivity to spiciness. *PLoS Biol* **16**, e2004921 (2018).
54. B. Becker, H. Mehlhorn, P. Andrews, H. Thomas, Ultrastructural investigations on the effect of praziquantel on the tegument of five species of cestodes. *Z. Parasitenkd.* **64**, 257–269 (1981).
55. P. Andrews, H. Thomas, The effect of praziquantel on *Hymenolepis diminuta* in vitro. *Tropenmed. Parasitol.* **30**, 391–400 (1979).
56. H. Thomas, R. Gonnert, R. Pohlke, J. Seubert, "Experimental and clinical studies with a new compound against tapeworms" in *Paper Read at the 2nd European Multi-Colloquy of Parasitology Trogir*, Yugoslavia, 1975), pp. 1–4.
57. H. Thomas, R. Gonnert, The efficacy of praziquantel against cestodes in cats, dogs and sheep. *Res. Vet. Sci.* **24**, 20–25 (1978).
58. Q. Liu *et al.*, Human sparganosis, a neglected food borne zoonosis. *Lancet Infect Dis* **15**, 1226–1235 (2015).
59. Y. Chen, X. Chen, H. Kang, Case report: Moving tumor-like foci behind refractory epilepsy-cerebral sparganosis successfully treated by surgery after failure of praziquantel treatment. *Front Neurol* **13**, 838849 (2022).
60. G. Bylund, B. Bang, K. Wikgren, Tests with a new compound (Praziquantel) against *Diphyllobothrium latum*. *J. Helminthol.* **51**, 115–119 (1977).
61. Norbury, Praziquantel use in aquaculture–Current status and emerging issues. *Int. J. Parasitol. Drugs Drug Resist.* **18**, 87–102 (2022).
62. A. Sitja-Bobadilla, M. C. de Felipe, P. Alvarez-Pellitero, In vivo and in vitro treatments against *Sparicotyle chrysophrii* (Monogenea: Microcotylidae) parasitizing the gills of gilthead sea bream (*Sparus aurata L.*). *Aquaculture* **261**, 856–864 (2006).
63. G. Schmahl, H. Mehlhorn, Treatment of fish parasites. 1. Praziquantel effective against Monogenea (*Dactylogyrus vastator*, *Dactylogyrus extensus*, *Diplozoon paradoxum*). *Z. Parasitenkd.* **71**, 727–737 (1985).
64. M. Woelfle *et al.*, Resolution of praziquantel. *PLoS Negl. Trop. Dis.* **5**, e1260 (2011).
65. P. Stothard, The sequence manipulation suite: JavaScript programs for analyzing and formatting protein and DNA sequences. *Biotechniques* **28**, 1102–1104 (2000).
66. G. M. Sastry *et al.*, Protein and ligand preparation: Parameters, protocols, and influence on virtual screening enrichments. *J. Comput. Aided Mol. Des.* **27**, 221–234 (2013).
67. Desmond Molecular Dynamics System, D. E. Shaw Research, New York, NY, 2021. *Maestro-Desmond Interoperability Tools*, Schrödinger,New York, NY 2021.